Global Environmental Science
www.sciltp.com/journals/ges

Article

Disturbance and Natural Recovery of Surface Water Quality in a Semi-Industrial Gold Mining District (Eséka, Central Cameroon): A Tropical Earth System Perspective

Irma Gaelle Awono [1], Moïse Welba [2], Rel Dechangue Tatou [1], Elisé Sababa [2,*] and Vincent Laurent Onana [1,2]

[1] Department of Geosciences and Environment, University of Ebolowa, Ebolowa P.O. Box 118, Cameroon
[2] Department of Earth Sciences, University of Yaoundé I, Yaoundé P.O. Box 812, Cameroon
* Correspondence: sababa.elise@facsciences-uy1.cm

How To Cite: Awono, I.G.; Welb, M.; Tatou, R.D.; et al. Disturbance and Natural Recovery of Surface Water Quality in a Semi-Industrial Gold Mining District (Eséka, Central Cameroon): A Tropical Earth System Perspective. *Glob. Environ. Sci.* **2026**, *2*(3), 372–391. https://doi.org/10.53941/ges.2026.100024

Publication History

Received: 25 June 2026
Revised: 18 August 2026
Accepted: 4 September 2026
Published:10 September 2026

Keywords

gold mining;
heavy metal contamination;
health risk;
natural restoration;
humid tropical setting

Highlights

- Semi-industrial gold mining in Eséka significantly degrades surface water quality
- High concentrations of Pb, Cd, As, Cr, and Co exceed WHO drinking water guidelines
- Water Quality Index (WQI) values range from good to very poor
- Ingestion is the dominant exposure pathway for heavy metals
- Older abandoned mining sites show natural restoration of water quality

Abstract: Surface water quality in the Eséka gold district (Central Cameroon) was investigated to understand the coupled impacts of semi-industrial mining and tropical Earth surface processes. Physicochemical parameters and heavy metal concentrations were quantified across a chronosequence of actively mined and abandoned sites. Mining activities significantly lowered water pH, increased water temperature, and reduced dissolved oxygen concentrations. High concentrations of Pb, Cd, As, and Cr are linked to sulfide oxidation and leaching of host minerals (e.g., galena, arsenopyrite) in waste rock. The Water Quality Index (WQI) ranges from good (at older, abandoned sites) to very poor (at active mines), suggesting that natural recovery processes may improve water quality at some mining sites in humid tropical environments. Health risk assessment identified ingestion as the primary exposure pathway. The cumulative Hazard Index (HI) for children was 29.55, indicating significant non-carcinogenic risk resulting from the combined contributions of Pb, As, Co, and Cr. Adults face elevated risks primarily from As and Co. These findings provide a conceptual model of mining-induced disturbance and natural attenuation in tropical catchments, with implications for global change remediation strategies and sustainable development in resource-dependent regions.

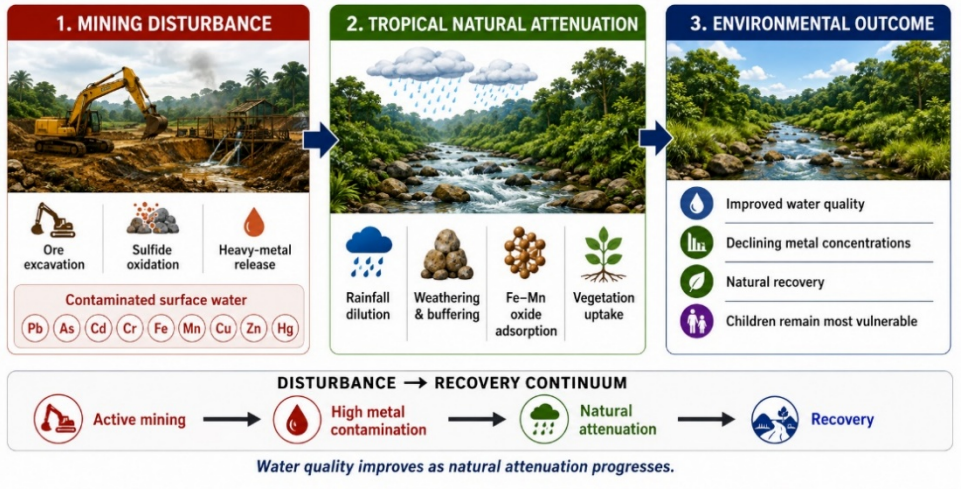

1. Introduction

Water is essential for life, human well-being, and economic development. However, global water resources are under increasing pressure from population growth, urbanization, industrialization, poor resource management, and climate change [1]. Among anthropogenic activities, mining, particularly gold mining, has emerged as a major threat to surface water quality, primarily through the release of heavy metals and toxic substances [2,3]. These contaminants not only degrade aquatic ecosystems [4] but also pose serious risks to human health, especially in developing countries where water treatment facilities are often lacking.

Cameroon, a Central African country where water availability varies considerably from one region to another and between the rainy and dry seasons, is no exception to this problem. Rapidly expanding artisanal and semi-industrial gold mining has led to documented cases of heavy metal contamination in rivers and streams, endangering local communities and biodiversity [3,5,6]. The Eséka gold district in Central Cameroon is characterized by significant semi-industrial gold mining activity [7]. While mining has brought economic benefits and livelihoods, it has also caused extensive landscape modification, sedimentation of watercourses, and potential contamination by toxic metals. Moreover, abandoned mining sites, now partly restored by natural vegetation, are still used by local populations for domestic and agricultural purposes, raising critical questions about water safety.

Although mining-related water pollution is well documented globally, e.g., [5,6,8–11], the trajectory of natural recovery in post-mining landscapes remains poorly constrained, particularly in humid tropical environments where rapid weathering can both mobilize and sequester contaminants. This study addresses three research questions: (i) To what extent does surface water quality recover following mine closure? (ii) Which potentially toxic elements persist in surface waters despite the cessation of mining activities? (iii) What are the implications of residual contamination for human health? The Eséka gold district offers a unique opportunity to investigate a disturbance-recovery continuum where active, abandoned, and older restored mining sites coexist within a small catchment. This setting allows us to ask: What is the timescale and mechanism of natural water quality restoration following semi-industrial gold mining in the tropics? Addressing this question moves beyond local assessment to inform Earth system science, specifically the coupling of anthropogenic land-use change with geochemical and hydrological cycles. Therefore, this study aims to: (1) characterize the physicochemical and heavy metal status of surface water across this disturbance gradient; (2) quantify pollution using multiple indices; (3) assess human health risks; and (4) develop a conceptual model of natural attenuation relevant to tropical mining regions globally.

2. Study Site

The study area lies in the Eséka municipality, Centre Region of Cameroon, between latitudes 3°24′15″ and 3°51′58″ N and longitudes 10°41′01″ and 10°57′31″ E. Some mining sites where both land and water extraction occurred have been abandoned for approximately 5–10 years (based on local interviews), whereas others remain active. Because the study sites share the same geological setting (migmatitic and lower gneisses), climatic conditions, and mining context, differences among sites are assumed to mainly reflect different stages of post-mining evolution, although local hydrological variability cannot be excluded.

Eséka has a tropical monsoon climate with four seasons, including two dry seasons and two rainy seasons. The average annual temperature is 25.5 °C, and annual rainfall is approximately 2126 mm. The study area is entirely dominated by dense and humid equatorial forest. This vegetation faces intense encroachment as a result of logging, farming, and mining. The hydrographic network is essentially dendritic and belongs to the catchment area of the Nyong River (Figure 1). Soils in the study area are ferralitic and hydromorphic.

The geology of the study area lies within the Nyong unit, which corresponds to the deeply restructured western part of the Ntem Complex [12]. This unit consists of metasedimentary and metaplutonic rocks emplaced 2050 Ma ago. It has been defined as a high-grade gneiss unit reactivated on the northwestern edge of the Congo Craton during the Neoproterozoic [13]. It outcrops mainly in the lower Nyong basin (Bas Nyong) between Eséka and Lolodorf and in the Edéa-Kribi region. It rests on the Congo Craton as an Eburnean Nappe [14], comprising both Archean and Palaeoproterozoic materials of volcano-sedimentary origin, including granulites, banded iron formations (BIF), plutonites (TTG, charnockites, dolerites, alkaline syenites), and greenstones (serpentinites, chlorite rocks). The lithological formations encountered in Eséka, and more specifically in the study area, are metamorphic. They are mainly composed of gneisses, micaschists, and schists (Figure 1). The local geology consists of granulitic orthogneisses with garnet-pyroxene, which cover a large part of the area, as well as migmatitic gneisses, magmatic amphibolic gneisses, micaschists and schists (Figure 1).

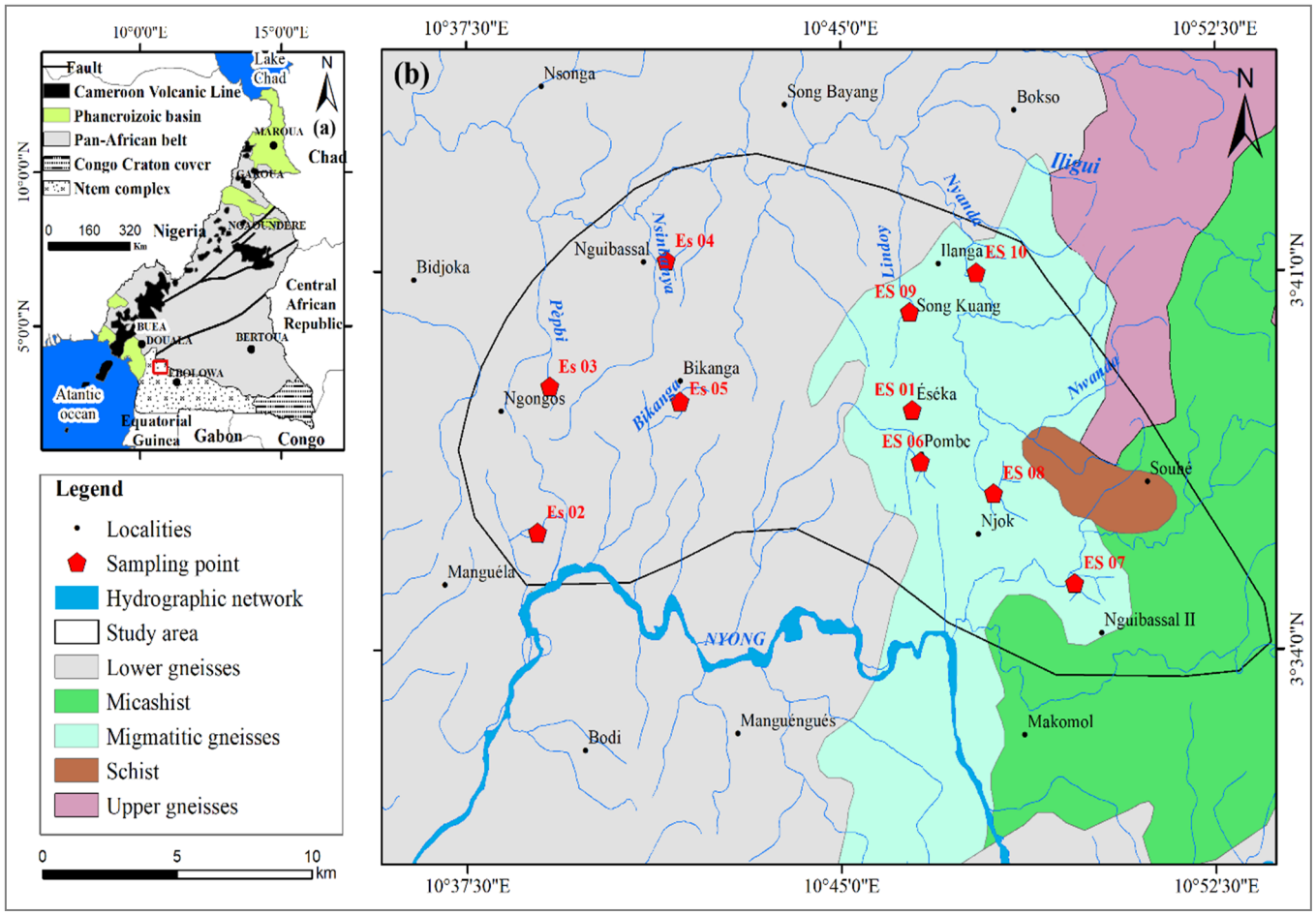

Figure 1. Location map of the study area: (**a**) the major geological units of Cameroon; (**b**) detailed geology of the study area [15].

3. Materials and Methods

3.1. Sampling Procedure

Samples were taken in accordance with the protocol developed by [16], which describes not only the procedure to be followed during sampling but also the steps involved in preparing the sampling materials. Water samples were collected using 1.5 L polyethylene bottles and then stored in an icebox at a temperature of 2 °C to ensure optimal preservation. A total of ten samples were collected, including four samples from watercourses, five samples from water at mine sites, and one sample from a well. The sampling sites were chosen based on their spatial distribution and proximity to mining operations.

3.2. Sample Analysis

Physicochemical parameters were determined both in the field and in the laboratory, rigorously following the methodological protocols recommended by [17,18]. Measurements of temperature (°C), pH, electrical conductivity (µS/cm), total dissolved solids (TDS in mg/L), and salinity (mg/L) were carried out using a LAQUA HORIBA PC 220 multi-parameter analyzer in accordance with ISO 10523 and NF 27888 standards. In the laboratory, analyses were performed within seven days of sampling. Dissolved oxygen (% saturation) was determined using a HACH HQ oximeter. Suspended solids content (SS) was determined directly using a HACH DR/2010 spectrophotometer (Hach Company, Loveland, CO, USA) at a wavelength of 810 nm. After calibrating the instrument at the indicated wavelength with distilled water, the spectrophotometric cell containing 10 mL of sample was introduced into the instrument to obtain a reading. Color was measured using a HACH DR/2010 spectrophotometer at a wavelength of 455 nm using 10 mL of sample, and the values obtained were expressed in platinum-cobalt (Pt-Co) units. Turbidity was measured using a HACH DR/2010 spectrophotometer at a wavelength of 450 nm using 10 mL of sample. The values obtained were expressed in formazine turbidity unit (FTU).

Calcium (Ca^{2+}) and magnesium (Mg^{2+}) concentrations were determined using a HACH DR 3900 UV–Vis spectrophotometer (Hach Company, Loveland, CO, USA), following the manufacturer's standard colorimetric procedure based on EDTA and EGTA complexation. Absorbance was measured at 522 nm, and concentrations were expressed in mg/L. The analytical performance characteristics, including the method detection limit, were those specified by the manufacturer for the corresponding HACH method.

 https://doi.org/10.53941/ges.2026.100024

The concentrations of dissolved metallic elements were determined by inductively coupled plasma optical emission spectrometry (ICP-OES) using a Perkin Elmer Optima 8000 spectrometer (PerkinElmer, Inc., Shelton, CT, USA), operated with WinLab 32 software, following filtration through Whatman paper (0.45 µm porosity), acidification with a drop of pure nitric acid, and storage at 0 to 4 °C. Quality control procedures included the analysis of procedural blanks, calibration verification standards, and replicate measurements. The calibration curves were established using certified multi-element standards, with linearity considered acceptable when $R^2 \geq 0.999$, in accordance with the procedure defined in [19]. Detection limits (LOD) were determined from blank measurements (3σ) and were typically in the range of 0.0004–0.03 mg L^{-1} for the analyzed elements. Analytical precision was controlled through replicate analyses (RSD < 5%), while recoveries of quality control standards were maintained between 90 and 110%. These procedures ensured the reliability of Fe, Mn, Cr, Co, and Cu determinations by ICP-OES according to NF ISO 11885 recommendations.

3.3. Analysis of Water Pollution

3.3.1. Water Quality Index (WQI)

The Water Quality Index is a synthetic method for classifying water potability based on the comparison of measured physicochemical parameters with international reference standards. This approach was initially developed by [20], and subsequently refined by [21]. In the present study, the WQI was used to assess the combined impact of natural and anthropogenic factors. The calculation of this index is based on the weighted arithmetic method described by [21], according to which a relative weight (Wi) is assigned to each parameter using the following formula:

$$Wi = k/Si$$

In this formula, "k" designates a constant of proportionality, which can be calculated according to the following equation:

$$k = 1/\Sigma(1/Si) \text{ [for i = 1 to n]}$$

"n" corresponds to the total number of parameters considered, while Si denotes the maximum value of the reference standard [22] for each parameter, expressed in mg/L, with the exception of pH, temperature (°C), and electrical conductivity (µS/cm).

Subsequently, a quality scale (Qi) is defined for each parameter by dividing its concentration (Ci in mg/L) by the respective standard (Si) and multiplying the result by 100, as shown in the following equation:

$$Qi = (Ci/Si) \times 100$$

The general WQI is then calculated as:

$$WQI = \Sigma(Wi \times Qi)/\Sigma Wi$$

Based on the classifications proposed by [23] and reiterated by [24], WQI values can be used to categorize water quality into five classes: <50 (excellent); 50–100 (good); 100–200 (poor); 200–300 (very poor); >300 (unfit for consumption).

3.3.2. Heavy Metal Pollution Index (HPI)

This index is used to assess the degree of contamination of water by toxic metals. It is calculated using the method proposed by [25], based on a weighted arithmetic mean. The relative weight (Wi) associated with each element is determined using the following formula:

$$Wi = K/Si$$

Where K is a constant (equal to 1 in this study), and Si represents the admissible standard limit of the parameters according to [22]. The second equation consists of determining the value of the sub-index (Qi) of the various parameters. The formula is as follows:

$$Qi = \Sigma(|Mi - Ii|)/(Si - Ii) \times 100$$

In this equation, Mi represents the measured value of the heavy metal; Ii represents the ideal value of the parameters (usually 0 for toxic metals); "Si" designates the standard value according to [22]. The final formula for the HPI is as follows:

$$HPI = \Sigma(Wi \times Qi)/\Sigma Wi$$

3.3.3. Heavy Metal Evaluation Index (HEI)

This index is calculated using the method described by [26] according to the following relationship:

$$HEI = \Sigma(Hc/HMAC)$$

Hc designates the observed concentration of the parameter, and HMAC represents the maximum authorized concentration for this parameter. For the purposes of this work, the MAC reference value aligns the drinking water quality standards established by the World Health Organization [22]. The HEI is used to classify the level of surface water pollution according to the following scale: HEI < 0.01, pollution is considered negligible; for HEI between 0.01 and 1, pollution remains low; HEI between 1 and 5 indicates moderate pollution; a value between 5 and 10 signals high pollution; HEI ≥ 10 reveals very high pollution [27].

3.3.4. Contamination Factor (CF)

The contamination factor is defined as the quotient of the concentration of a specific metal (Cn) and its natural background (Bn). This index is used to assess the level of metal contamination in water.

$$CF = Cn/Bn$$

In this equation, Cn represents the observed concentration of element ''n'', while Bn indicates the background value corresponding to its natural level in the environment. The latter has been standardized to the reference data proposed by the WHO [22]. According to the classification proposed by [28], four levels of contamination can be distinguished based on the contamination factor (CF) values: CF < 1 indicates low contamination, between 1 and 3 moderate contamination, between 3 and 6 considerable contamination, and CF ≥ 6 indicates very high contamination.

3.3.5. Degree of Contamination Index (DCI)

The degree of contamination is calculated by summing the contamination factor (CF) values.

$$DCI = \Sigma\ CF$$

DCI values > 5 indicate a considerable degree of contamination, and conversely, DCI < 5 indicate a low degree of contamination.

3.3.6. Pollution Load Index (PLI)

Developed by [29], the pollution load index (PLI) is determined as the root of the product of ''n'' concentration factors. It provides a synthetic and comparative method for assessing the level of metal pollution, particularly in soil and water [30].

$$PLI = \sqrt[n]{(CF_1 \times CF_2 \times CF_3 \times \ldots \times CF_n)}$$

PLI > 1 indicate pollution and conversely, PLI <1 indicates the absence of pollution [28,31].

3.4. Human Health Risk Assessment Model

The [32] risk assessment method was used to understand the impact of heavy metals on human health. Two principal exposure routes (ingestion and dermal absorption) were investigated in this study to assess non-carcinogenic risks. The level of risk varies according to various parameters such as duration of exposure, body weight, lifestyle, individual tolerance, and daily practices. Ingestion is the principal exposure pathway, followed by dermal absorption, which is especially significant for children. In order to determine the non-carcinogenic risk, the average daily dose (ADD) was calculated.

$$ADD\_ingestion = (C \times IR \times EF \times ED)/(BW \times AT)$$

$$ADD\_dermal = (C \times SA \times Kp \times ET \times EF \times ED \times CF)/(BW \times AT)$$

ADD ingestion and ADD dermal represent the average daily doses by ingestion and dermal absorption, respectively, for a given heavy metal. The concentration (C) is expressed in mg/L, while the skin permeation coefficient (Kp) (cm/h) depends on the metal. The ingestion rate (IR) represents the average amount of water in liters consumed per day. The exposed skin area (SA) (cm^2) and exposure time (ET) (hours/day) define the extent of contact, modulated by frequency (EF) (days/year) and exposure duration (ED) (years). A conversion factor (CF = 0.001) is used to convert mg/L to mg/cm^3. Body weight (BW) is expressed in kilograms. Finally, the average exposure time (AT) (days) corresponds to non-carcinogenic risks to ED × 365. The values for some of these parameters are listed in Tables 1 and 2.

The mean concentrations of Hg, Cd, Zn, Pb, As, Co, Cu, Fe, Mn, and Cr were used. Based on ADD ingestion and ADD dermal, hazard quotients (HQ) were computed. The HQ represents the ratio of the estimated exposure dose to the corresponding reference dose (RfD) [32].

$$HQ = ADD/RfD$$

The sum of all HQ values provides the Hazard Index (HI), which estimates the potential cumulative non-carcinogenic risk associated with multiple exposure pathways under standard exposure assumptions. An HQ or HI value > 1 indicates the potential for adverse health effects but should not be interpreted as direct evidence of health impacts, as actual risks depend on local water-use practices, exposure frequency, and population characteristics. Carcinogenic risk was not assessed because the required slope factor values were unavailable for several analyzed metals, preventing a consistent risk evaluation.

Table 1. parameters associated with average daily doses via ingestion and dermal absorption for a given heavy metal.

Adult							
IR	EF	ED	BW	AT	SA	ET	CF
2	350	30	70	10,950	18,000	0.5	0.001
Children							
IR	EF	ED	BW	AT	SA	ET	CF
1	350	6	15	2190	6600	0.5	0.001

IR: ingestion rate (L/day); EF: frequency (days/year); ED: exposure duration (years); BW: body weight (kg); AT: exposure time (days); SA: exposed skin area (cm^2); ET: exposure time (hours/day); CF: conversion factor (0.001) used to convert mg/L to mg/cm^3.

 https://doi.org/10.53941/ges.2026.100024

Table 2. Toxicological parameters used for non-carcinogenic human health risk assessment through ingestion and dermal exposure.

Metal	RfD Ingestion (mg/kg·day)	RfD Dermal (mg/kg·day)	ABS Dermal (Fraction)	Kp (cm/h)
Hg	0.0003	0.00021	0.001	0.001
Cd	0.001	0.0001	0.001	0.0001
Zn	0.3	0.06	0.001	0.0006
Pb	0.0035	0.000525	0.001	0.000042
As	0.0003	0.00012	0.03	0.001
Co	0.0003	0.00006	0.01	0.0003
Cu	0.04	0.012	0.001	0.001
Fe	0.7	0.14	0.001	0.0001
Mn	0.14	0.004	0.001	0.0001
Cr	0.003	0.0006	0.01	0.002

RfD ingestion, oral reference dose (mg/kg·day); RfD dermal, dermal reference dose (mg/kg·day); ABS dermal, dermal absorption factor (fraction); Kp, dermal permeability coefficient (cm/h).

4. Results

4.1. Landscape Characteristics

Field observations indicate that the landscape at the Eséka mining sites is characterized by mounds of excavated earth/soil, artisanal mining pits, and washing ponds. Extraction activities at the mining sites characteristically migrate inland from the riverbanks, leading to the involvement of artisanal miners in quarrying operations. The excavation of pits and ditches can contribute to deforestation and the loss of plant cover, as observed at all the analyzed sites. Prospecting and ore extraction activities degrade soil quality. The necessary process of waste rock removal to expose the gravel causes ecological imbalances. During various field visits, mine drainage was observed to have affected the area, mainly because the deposits generally mined are surface deposits. Some mining sites where both land and water extraction occurred have now been abandoned, leaving behind pools that were previously used as washing areas. Farmers use the water to irrigate their salad gardens. The following images were taken on site to show the current state of the landscape (Figure 2).

Figure 2. Environmental degradation as a result of artisanal mining in the study area.

4.2. Physico-Chemical Parameters of Surface Water

Eleven (11) physicochemical parameters were determined in this study: pH, electrical conductivity (EC), temperature, total dissolved solids (TDS), salinity, dissolved oxygen (DO), total suspended solids (TSS), color, turbidity, and calcium and magnesium ions.

4.2.1. Hydrogen Potential (pH)

pH values showed limited spatial variability among the three sampling sites (Figure 3a). The lowest value was recorded in the well (5.84), while the river water (mean = 6.41) was slightly below the WHO and ANOR recommended range of 6.5-9.0. In contrast, the water at the mining site (mean = 6.56) remained within the recommended range (Table 3).

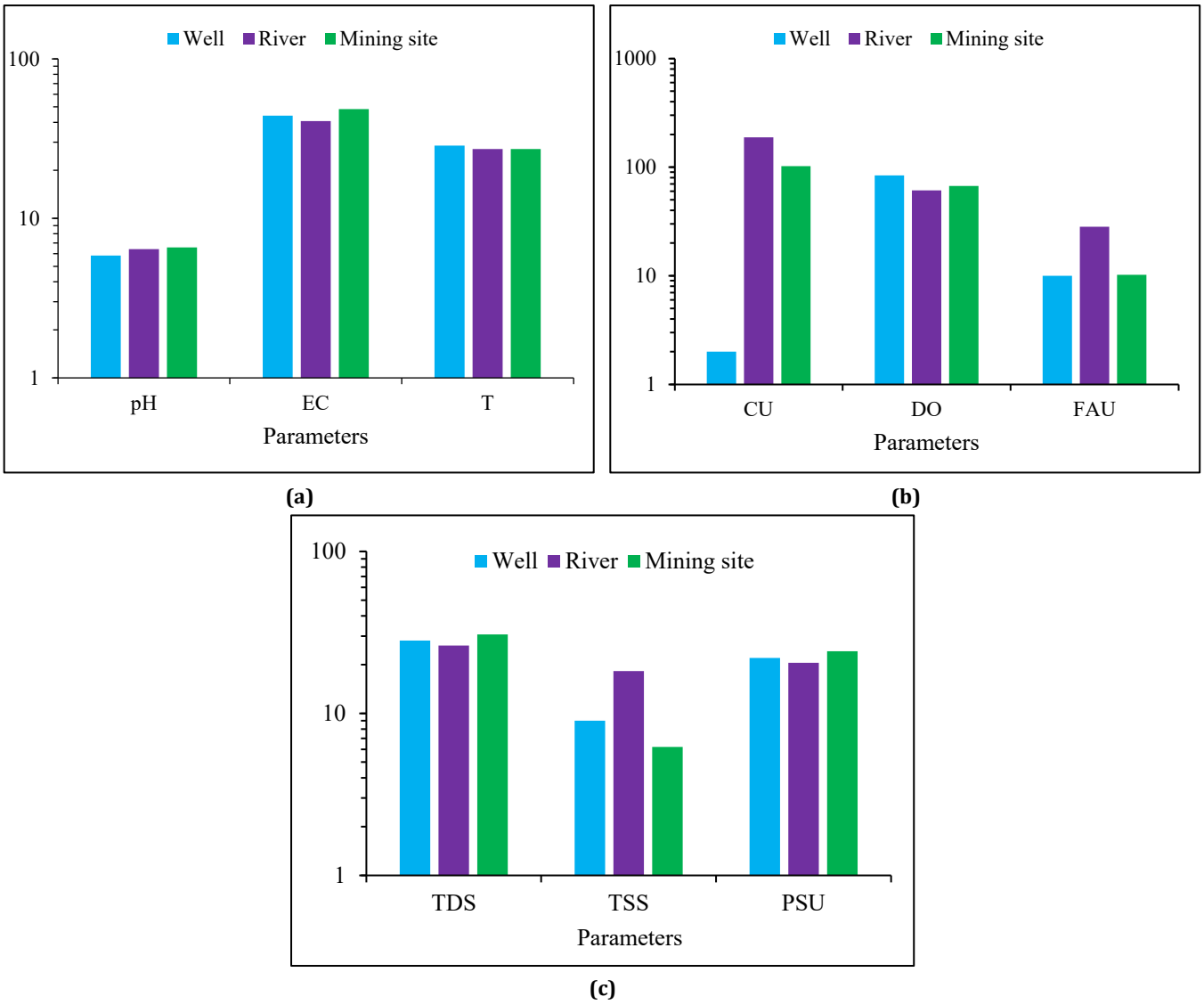

Figure 3. Distribution of physico-chemical parameters in well water, river water and mine water: (**a**) pH, EC (µS/cm), T (°C); (**b**) CU (Pt.Co), DO (%), FAU (FTU); (**c**) TDS (mg/L), TSS (mg/L), PSU (mg/L).

Table 3. Summary of physicochemical parameters and heavy metal concentrations measured in surface waters from the study area.

	Unit	Reference		Well	River			Mining Site		
		ANOR	WHO		Min	Max	Average	Min	Max	Average
pH	-	6.5–9.0	6.5–8.5	5.84	5.91	6.84	6.41	6.42	6.94	6.56
EC	µS/cm	-	<1500	44.00	22.00	84.00	41.00	34.00	86.00	48.00
T	°C	25	<25	28.60	25.70	30.40	27.18	26.10	29.50	27.22
PSU	mg/L		-	22.00	11.00	42.00	21.00	17.00	43.00	24.00
TDS	mg/L	-	1	28.16	14.08	53.76	26.24	21.76	55.04	30.72
DO	%	-	-	83.80	11.40	83.30	61.03	45.20	86.10	67.10
CU	Pt.Co	15.00	15.00	2.00	83.00	282.00	188.00	33.00	184.00	102.00

 https://doi.org/10.53941/ges.2026.100024

Table 3. *Cont.*

	Unit	Reference		Well	River			Mining Site		
		ANOR	WHO		Min	Max	Average	Min	Max	Average
TSS	mg/L	-	5.00	9.00	7.00	38.00	18.25	4.00	13.00	6.20
FAU	FTU	2	1–5	10.00	10.00	66.00	28.25	2.00	32.00	10.20
Ca^{2+}	mg/L	-	75–200	1.02	0.78	3.54	1.79	1.39	3.38	2.26
Mg^{2+}	mg/L	50	150	1.35	0.76	1.80	1.25	1.12	1.31	1.21
Cr	mg/L	0.05	0.05	0.06	0.03	0.11	0.07	0.03	0.09	0.06
Mn	mg/L	0.05	0.40	0.005	0.40	1.30	0.78	0.10	0.90	0.38
Fe	mg/L	0.2	0.3	0.27	1.32	3.11	2.13	0.79	3.14	1.33
Cu	mg/L	-	2.00	0.09	0.18	4.17	1.92	0.43	2.20	1.29
Hg	mg/L	-	0.006	0.001	0.001	0.004	0.003	0.0008	0.004	0.002
Cd	mg/L	0.005	0.003	0.002	0.0006	0.009	0.0053	0.0031	0.008	0.0056
Zn	mg/L	5.00	5.00	0.60	1.68	3.70	2.75	1.55	4.00	2.17
Pb	mg/L	0.05	0.01	0.03	0.04	0.08	0.06	0.02	0.55	0.14
As	mg/L	0.05	0.01	0.04	0.01	0.03	0.02	0.02	0.09	0.06
Co	mg/L		0.05	0.02	0.02	0.083	0.055	0.03	0.22	0.08

pH (Potential of Hydrogen): Measures the acidity or alkalinity of a solution (scale from 0 to 14). EC (Electrical Conductivity): The ability of a solution to conduct electricity, expressed in µS/cm or mS/cm. T (Temperature): Measures the heat level of water, influencing gas solubility and biological activity. PSU (Practical Salinity Unit): A unit of salinity indicating the concentration of dissolved salts in water. TDS (Total Dissolved Solids): The total amount of dissolved minerals, salts, and organic matter in water. DO (Dissolved Oxygen): The amount of oxygen available in water, essential for aquatic life. CU (Color Unit): A measure of water color, often caused by dissolved organic matter or metals. TSS (Total Suspended Solids): The solid particles which remain suspended in water rather than dissolving. FAU (Formazine Attenuation Units): A turbidity unit used to measure water clarity.

4.2.2. Electrical Conductivity (EC)

Electrical conductivity remained low across all sampling sites, ranging from 22 to 86 µS/cm, well below the WHO guideline value of 1500 µS/cm. Mean EC values were 41 µS/cm for river water, 48 µS/cm for mine-site water, and 44 µS/cm for well water (Table 3).

4.2.3. Temperature

The water temperature ranged from 25.7 to 30.4 °C, with average values of 27.18 °C for river water and 27.22 °C for water from the mining site, while the temperature of well water reached 28.6 °C. All measured temperatures exceeded the reference value of 25 °C, although only slight spatial variations were observed (Figure 3a).

4.2.4. Salinity

Salinity varied only slightly among sampling environments, ranging from 11 to 43 mg/L. Mean values were 21 mg/L for river water, 24 mg/L for mine-site water, and 22 mg/L for well water, all remaining below the WHO guideline value (Table 3).

4.2.5. Total Dissolved Solids (TDS)

TDS concentrations followed a pattern similar to EC (Figure 3c). Mean TDS values were highest in mine-site water (30.72 mg/L), followed by well water (28.16 mg/L) and river water (26.24 mg/L), while remaining below the WHO guideline limit (Table 3).

4.2.6. Dissolved Oxygen Saturation (DO)

The dissolved oxygen saturation ranged from 11.4 per cent to 86.1 per cent. The DO value in the well is 83.8 per cent, whilst the average dissolved oxygen values are 61.03 per cent in river water and 67.1 per cent in water from the mining site (Table 3).

4.2.7. Color

Color exhibited marked spatial variability. Values ranged from 33 to 184 Pt-Co in mine-site water and from 83 to 282 Pt-Co in river water, with mean values of 102 and 188 Pt-Co, respectively. The well water showed a markedly lower value (2 Pt-Co). Most of the surface water samples exceeded the reference values (Table 3).

4.2.8. Total Suspended Solids (TSS)

Total Suspended Solids (TSS) value in well water was 9 mg/L. In contrast, in river water, TSS values ranged from 7 to 38 mg/L, with an average of 18.25 mg/L. Values obtained in mine site water ranged from 4 to 13 mg/L, with an average of 6.2 mg/L. Maximum values are recorded in river water (Figure 3c). In comparison with the optimal values recommended by the WHO, these different values are either higher or lower than the standards.

4.2.9. Turbidity (FAU)

The turbidity value obtained in the well water is 10 FTU. In rivers, the turbidity value increases and varies from 10 to 66 FTU with an average of 28.25 FTU. In water

from mining sites, the turbidity value obtained varies between 2 and 32 FTU, with an average of 10.20 FTU. The maximum values were recorded in river water (Figure 3b). Most of the turbidity readings measured in the various environments do not meet the standard drinking water guidelines established by the WHO and ANOR (Table 3).

4.2.10. Calcium and Magnesium Ions

Calcium concentrations ranged from 0.78 to 3.54 mg/L in river water, 1.39 to 3.38 mg/L in mine-site water, and 1.02 mg/L in well water. Magnesium concentrations showed limited variability, ranging from 0.76 to 1.80 mg/L across all sampling environments, with mean values close to 1.3 mg/L. Calcium levels were below the range recommended by the WHO and ANOR, while magnesium levels remained within acceptable limits (Table 3).

4.3. Concentrations of Heavy Metals

This study analyzed ten (10) trace metals (TMEs), including Cr, Mn, Fe, Cu, Hg, Cd, Zn, Pb, As, and Co.

Chromium (Cr): concentration in well water is 0.06 mg/L. In river water, it varies from 0.03 to 0.11 mg/L, with an average of 0.07 mg/L. At mine sites, concentrations fluctuate between 0.03 and 0.09 mg/L, with an average of 0.06 mg/L. Across the three environment types, these values consistently exceed the thresholds recommended by the WHO and ANOR (Table 3). The highest Cr concentrations were found in the northern and western sectors of the study area (Figure 4).

Manganese (Mn): not detected in the well water. In river water, the concentration ranges from 0.4 to 1.30 mg/L, with an average of 0.78 mg/L. For water from mining sites, it ranges from 0.10 to 0.90 mg/L, with an average of 0.38 mg/L (Table 3). The highest concentrations of Mn were found in river water, particularly in the northern and western zones, which are similar to Cr behavior (Figure 4).

Iron (Fe): concentration in the well water is 0.27 mg/L. In rivers, concentrations range from 1.32 to 3.11 mg/L, with an average of 2.13 mg/L. At mine sites, concentrations range from 0.79 to 3.14 mg/L, with an average of 1.33 mg/L. Maximum Fe concentrations are recorded in river water, located to the north-west and south of the study area (Figure 4). Only well water has a concentration close to the reference value limit.

Copper (Cu): concentration is low in the well water (0.09 mg/L). In river water, concentrations range from 0.18 to 4.17 mg/L, with an average of 1.92 mg/L. At mine sites, concentrations ranged from 0.43 to 2.20 mg/L, with an average of 1.29 mg/L. The highest Cu concentrations are found in the western part of the study area (Figure 4). However, in all environments, concentrations remained below WHO thresholds (Table 3).

Mercury (Hg): in well water, the mercury concentration is 0.001 mg/L. In river water, it varies between 0.001 and 0.004 mg/L, with an average of 0.003 mg/L. Water from mining sites has values between 0.0008 and 0.004 mg/L, with an average of 0.002 mg/L (Table 3). The highest concentrations are found in rivers, particularly towards the west and south of the sector (Figure 4).

Cadmium (Cd): concentration is low in well water (0.002 mg/L). In rivers, it varies between 0.0006 and 0.009 mg/L, with an average of 0.0053 mg/L. At mine sites, it fluctuates between 0.0031 and 0.008 mg/L, with an average of 0.0056 mg/L. The highest concentrations are found at mining sites, mainly to the west and south of the study area. Most Cd values are close to those of ANOR.

Zinc (Zn): the concentration of zinc in well water is 0.6 mg/L. It varies from 1.68 to 3.70 mg/L in rivers (mean: 2.75 mg/L) and from 1.55 to 4 mg/L in mine sites (mean: 2.17 mg/L). All observed values are below the thresholds set by the WHO and ANOR (Table 3). The highest concentrations were found towards the south and east of the study area (Figure 4).

Lead (Pb): Lead concentrations exceeded WHO limits (0.01 mg/L) in all environments, with the highest mean at mine sites (0.14 mg/L) and a maximum of 0.55 mg/L. This spatial trend (active mines > rivers > well) directly links Pb enrichment to current mining operations (Table 3).

Arsenic (As): Arsenic concentrations follow this pattern: mining sites (average of 0.06 mg/L) > wells (0.04 mg/L) > waterways (0.02 mg/L), all of which exceed the WHO limit of 0.01 mg/L but vary in relation to the value defined by ANOR (Table 3). (Table 3). The highest concentrations were found at the mining sites, located in the extreme west and center of the study area (Figure 4).

Cobalt (Co): the cobalt concentration in well water is 0.02 mg/L. In rivers, it varies from 0.02 to 0.083 mg/L (mean: 0.055 mg/L), while at mine sites it fluctuates from 0.03 to 0.22 mg/L (mean: 0.08 mg/L). Although some Co concentrations were below the WHO reference value of 0.05 mg/L, the mean concentrations in river and mining-site waters exceeded this value (Table 3). The highest concentrations were observed at the mining sites located in the eastern and western parts of the study area (Figure 4).(Table 3). Maximum concentrations were observed at the mining sites, located to the east and west of the survey area (Figure 4).

 https://doi.org/10.53941/ges.2026.100024

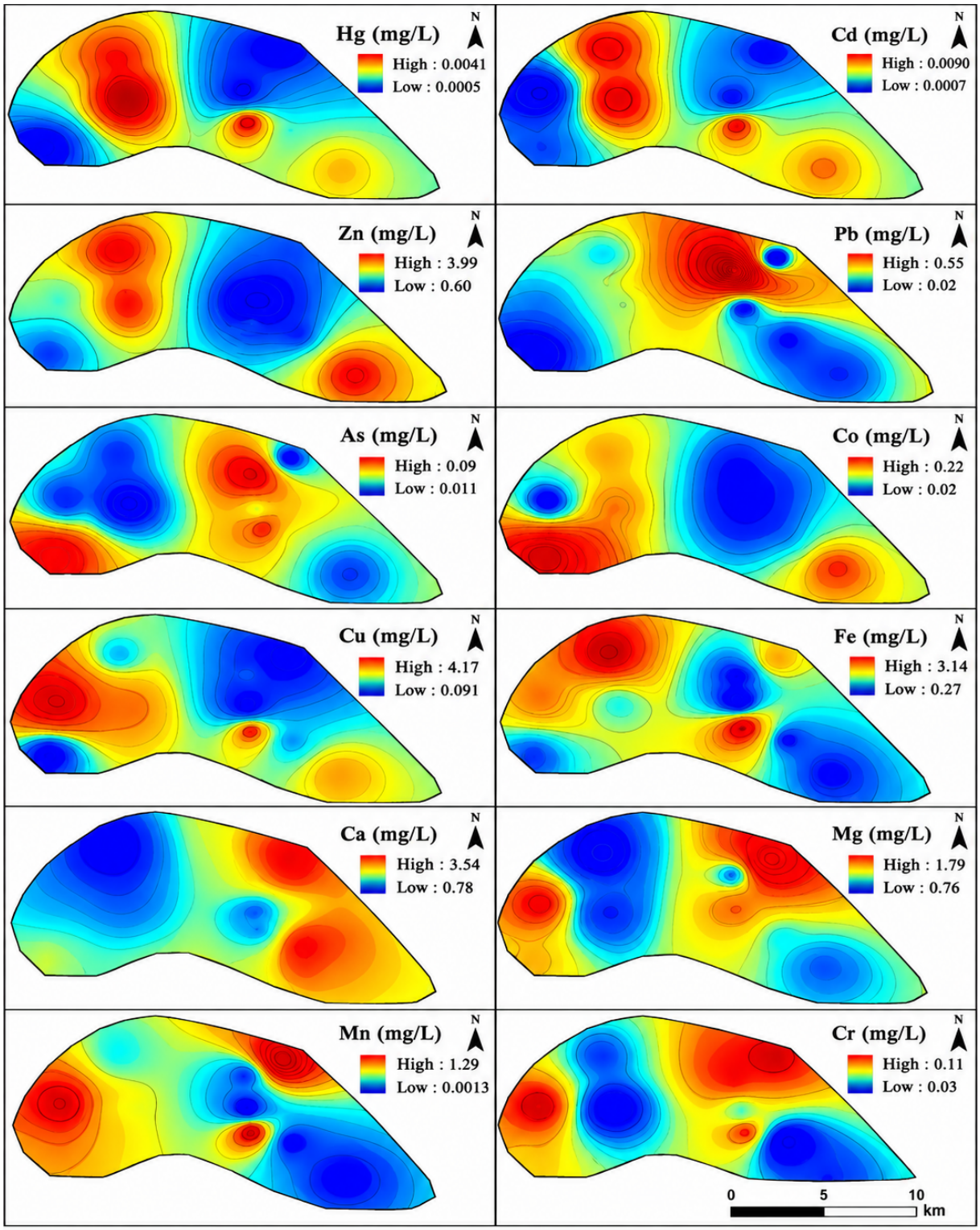

Figure 4. Spatial distribution of chemical element values in the study area.

4.4. Water Pollution Indices

Several pollution indices (CF, PLI, DCI, HEI, HPI and WQI) were used to provide a complementary assessment of surface water quality and metal contamination. While some indices show partial overlap, they highlight different aspects of pollution: WQI reflects overall water quality, whereas the other indices focus on the level and cumulative impact of heavy metal contamination.

4.4.1. Contamination Factor (CF), Pollution Load Index (PLI) and Degree of Contamination Index (DCI)

The graphical representation of CF and the data for the various indices are shown in Figure 5 and Table 4. Heavy metals such as Mn (0), Fe (0.90), Cu (0.05), Hg (0.08), Cd (0.67), Zn (0.12) and Co (0.4) in the well water have a contamination factor (CF) less than 1, indicating low contamination by these elements (Figure 5a). In contrast,

Cr and Pb reveal moderate contamination, with CF values of 1.20 and 2.5, respectively (Table 4). The arsenic (As) contamination factor was 4, indicating significant contamination of the well water by this element.

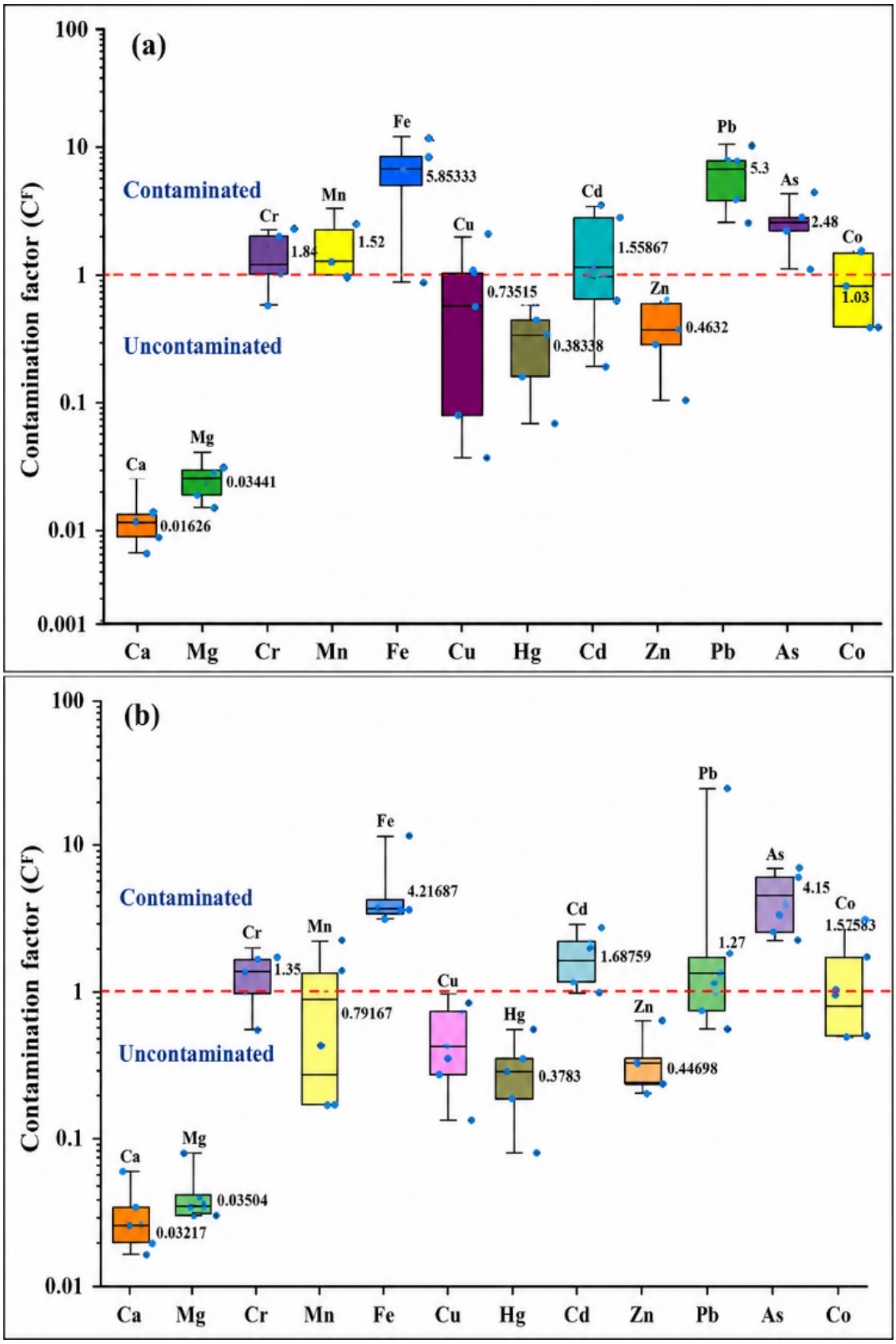

Figure 5. Variation in contamination factor (CF): (**a**) in river and well water, (**b**) in mine site water (the Pb value has been divided by 3).

The river water shows relatively low levels of Cu, Hg and Zn contamination, with average CF of 0.96, 0.46 and 0.55, respectively (Figure 5a). In contrast, Cr, Mn, Cd, As and Co indicate moderate contamination, with average contamination factors of 1.45, 1.94, 1.78, 2.10 and 1.10 respectively (Table 4). Finally, Fe and Pb concentrations

 https://doi.org/10.53941/ges.2026.100024

reach critical levels, with contamination factors of 7.09 and 6, indicating extremely high pollution of the river water by these elements. The PLI shows values greater than 1 for Cr (1.21), Mn (1.56), Fe (4.61), Cd (1.17), Pb (4.06), and As (1.73), reflecting pollution of the river water by these elements. Regarding the degree of contamination index (DCI) in river water, a fairly considerable degree of contamination is observed in Cr (5.80), Mn (7.75), Fe (28.37), Cd (7.13), Pb (24.0) and As (8.40).

Table 4. Contamination factor (CF) pollutant load index (PLI) and degree of contamination index (DCI) in surface water in the study area.

	Well	River					Mining Site				
	CF	CF			PLI	DCI	CF			PLI	DCI
		Min	Max	Average			Min	Max	Average		
Cr	1.20	0.60	2.20	1.45	1.21	5.80	0.60	1.80	1.28	1.19	6.40
Mn	0.00	1.00	3.25	1.94	1.56	7.75	0.25	2.25	0.95	0.64	4.75
Fe	0.90	4.40	10.37	7.09	4.61	28.37	2.63	10.47	4.44	3.78	22.20
Cu	0.05	0.09	2.09	0.96	0.65	3.83	0.22	1.10	0.64	0.56	3.22
Hg	0.08	0.20	0.68	0.46	0.50	1.83	0.13	0.63	0.38	0.33	1.88
Cd	0.67	0.23	3.00	1.78	1.17	7.13	1.03	2.63	1.79	1.70	8.93
Zn	0.12	0.34	0.74	0.55	0.59	2.20	0.31	0.80	0.43	0.41	2.17
Pb	2.50	3.50	7.50	6.00	4.06	24.0	2.00	55.0	14.46	6.72	72.30
As	4.00	1.10	2.70	2.10	1.73	8.40	2.40	9.00	5.64	5.06	28.20
Co	0.40	0.40	1.66	1.10	0.96	4.40	0.52	4.40	1.62	1.11	8.10

At the mining sites, the average CF for Mn (0.95), Cu (0.64), Hg (0.38) and Zn (0.43) remains below 1 (Figure 5b), indicating very low contamination of the water by these elements. On the other hand, Cr, Cd, and Co have mean CF values of 1.28, 1.79 and 1.62 respectively, placing them in the category of moderately contaminated water.

Additionally, the average CF of Fe (4.44) and As (5.64) indicate highly contaminated water, characterized by a CF between 3 and 6. Finally, Pb has a particularly high CF value, indicating significant contamination of mine site water by this element. The Pollution Load Index (PLI) shows average values in excess of 1 for Cr (1.19), Fe (3.78), Cd (1.70), Pb (6.72), As (5.06) and Co (1.11), highlighting water pollution at mining sites by these elements (Table 4). In addition, the Degree of Contamination Index (DCI) reveals a significant level of contamination, with respective values of 6.40 for Cr, 22.20 for Fe, 8.93 for Cd, 72.30 for Pb, 28.20 for As and 8.10 for Co (Table 4). These results indicate a high level of contamination in water from mining sites (Figure 5).

4.4.2. Heavy Metal Evaluation Index (HEI)

The data from the Heavy Metal Evaluation Index (HEI) show significant disparities depending on the sampling environment, as shown in Table 5. Analysis of the well water produced HEI of 9.92, placing it in the category of water with high metal pollution. The Pèpbi River recorded an HEI value of 24.01.

Table 5. Heavy metal pollution index (HPI), Water quality index (WQI) and Heavy metal evaluation index (HEI) in surface water obtained from heavy metals.

Samples	Sites	Longitudes	Latitudes	HPI	WQI	HEI
ES 01	Well	10.77362	3.64033	123.39	103.48	9.92
ES 02	Manguéla mining site	10.64853	3.60276	213.90	159.88	23.09
ES 03	River Pèpbi	10.65268	3.64775	144.50	290.72	24.01
ES 04	River Nsimbanya	10.69167	3.68644	275.61	218.01	28.17
ES 05	River Bikanga	10.69617	3.64311	272.93	117.44	21.94
ES 06	Pombe mining site	10.77632	3.62435	299.69	280.71	31.30
ES 07	Nguibassal mining site	10.82777	3.58688	208.19	120.48	17.68
ES 08	Njok mining site	10.80086	3.61459	199.82	85.55	15.32
ES 09	Song-Kuang Mining site	10.77289	3.67052	916.17	173.74	70.77
ES 10	River Nwanda	10.79505	3.68266	143.01	274.10	19.58

This is higher than 10, which means that the water from this river is highly polluted with heavy metals. The highest HEI value in the rivers was measured in the Nsimbanya river, with a value of 28.17. The water from this river is affected by heavy metal pollution. As for the Bikanga river, its HEI of 21.94 places it in the category of water highly polluted with heavy metals. For the Nwanda river, the index is 19.58, also indicating water heavily polluted with heavy metals.

At the Manguéla mining site, the HEI reached 23.09, which corresponds to poor water that is highly polluted with heavy metals. At the Pombe mining site, the HEI was particularly high at 31.30, classifying it as water highly

polluted with metallic elements. In the case of the Nguibassal and Njok mining sites, the index value are 17.68 and 15.32, respectively, confirming that the water is highly contaminated with heavy metals according to the critical limit. Lastly, the Song-Kuang mining site is the one with the highest HEI value. This site showed an index of 70.77, indicating extremely high heavy metal pollution.

4.4.3. Water Quality Index (WQI)

The results obtained from the water quality index (WQI) show significant variations depending on the sampling environment, as shown in Table 5. Analysis of the well water reveals a Water Quality Index (WQI) of 103.48, a value which classifies this water as 'poor quality' according to the established thresholds. The highest WQI value was recorded for water from the River Pèpbi, at 290.72, followed by the Nwanda River at 274.10, and the Nsimbanya River with a WQI of 218.01; these fall within the 200–300 range and are therefore classified as 'very poor quality'. As for the River Bikanga, the measured index is 117.44, which also corresponds to poor water quality. The descending order of river water pollution, according to the WQI, is as follows: Pèpbi river > Nwanda river > Nsimbanya river > Bikanga river. The WQI values for the mining sites range from 85.55 to 280.71. The Manguéla mining site has a WQI of 159.88, placing it in the poor-water quality category. A significantly high value is observed at the Pombe mining site, with a WQI of 280.71, placing this water in the very poor-quality class, in line with the 200 to 300 range. The water sampled at the Nguibassal mine site shows a WQI of 120.48, also placing it in the poor-quality category. Conversely, the Njok mine site shows a more moderate value of 85.55, belonging to the good-water quality category (WQI between 50 and 100). Finally, the Song-Kuang mine site recorded a WQI of 173.74, which places it in the poor-water quality category.

4.4.4. Integration between the Different Indices and limitations

A synthesis of the five indices (CF, PLI, DCI, HEI, HPI and WQI) reveals strong internal consistency (Tables 4 and 5, Figure 5). All indices classify active mining sites (e.g., Pombe, Song-Kuang) as highly to extremely polluted, while the abandoned Njok site consistently falls into good or low pollution categories. This convergence across independent metrics strengthens the conclusion that water quality improves with site age, pointing to natural attenuation.

The strong correlation between WQI, HEI, DCI, and PLI indicates that for this data set, any single index would suffice for management decisions. However, a critical limitation is that all indices assume additive toxicity and equal weight for each parameter, which is ecotoxicologically unrealistic. Furthermore, they do not account for metal speciation or bioavailability. For example, while total As is high, the proportion present as the more toxic As(III) vs. As(V) is unknown. Future work should integrate speciation analysis to refine risk estimates.

4.5. Assessment of Health Risks to the Local Population

The results in Table 6 show that, for most heavy metals, the average daily intake (ADD ingestion) values exceed the reference doses (RfD). This trend is observed for children for Zn, Pb, As, Co, Cu, Fe, Mn and Cr, and for adults for As and Co, suggesting a potential health risk associated with consumption. On the other hand, ADD dermal values are consistently below RfDs for both adults and children, indicating that dermal exposure does not pose a significant non-carcinogenic threat in the study area. The calculation of the hazard quotient (HQ) confirms these observations in Table 5 and Figure 6. The HQs for ingestion show critical values for several metals such as Pb (1.80), As (8.65), Co (13.74), Cu (2.27), and Cr (1.43) for children, and As (3.70) and Co (5.89) for adults. In contrast, HQs derived from dermal exposure remain below the threshold of 1, indicating no harmful risk. Finally, the hazard index (HI) serves as an overall indicator of cumulative risk. The HI values for ingestion reach 12.65 for adults and 29.55 for children, indicating a high potential for chronic non-carcinogenic effects. Conversely, skin contact HI values remain very low (1.95E-03 for adults and 3.33E-03 for children), confirming the absence of risk via the dermal route (Figure 6e).

Table 6. Potential health risks from heavy metals in the study area.

	ADDi (mg/kg/day)		ADDd (mg/kg/day)		Hazard Quotient (HQ) by Ingestion		Hazard Quotient (HQ) by Dermal	
	Children	Adult	Children	Adult	Children	Adult	Children	Adult
Hg	0.00015	0.00006	4.81×10^{-10}	2.81×10^{-10}	0.49	0.21	2.29×10^{-6}	1.34×10^{-6}
Cd	0.00032	0.00014	1.06×10^{-10}	6.19×10^{-11}	0.32	0.14	1.06×10^{-6}	6.19×10^{-7}
Zn	0.14345	0.06143	2.84×10^{-7}	1.66×10^{-7}	0.48	0.20	4.73×10^{-6}	2.77×10^{-6}
Pb	0.00632	0.00270	8.75×10^{-10}	5.12×10^{-10}	1.80	0.77	1.67×10^{-6}	9.74×10^{-7}
As	0.00260	0.00111	2.57×10^{-7}	1.50×10^{-7}	8.65	3.70	2.14×10^{-3}	1.25×10^{-3}
Co	0.00412	0.00177	4.08×10^{-8}	2.39×10^{-8}	13.74	5.89	6.80×10^{-4}	3.98×10^{-4}
Cu	0.09065	0.03882	2.99×10^{-7}	1.75×10^{-7}	2.27	0.97	2.49×10^{-5}	1.46×10^{-5}
Fe	0.09870	0.04227	3.26×10^{-8}	1.90×10^{-8}	0.14	0.06	2.33×10^{-7}	1.36×10^{-7}

 https://doi.org/10.53941/ges.2026.100024

Table 6. *Cont.*

	ADDi (mg/kg/day)		ADDd (mg/kg/day)		Hazard Quotient (HQ) by Ingestion		Hazard Quotient (HQ) by Dermal	
	Children	Adult	Children	Adult	Children	Adult	Children	Adult
Mn	0.03196	0.01369	1.05×10^{-8}	6.16×10^{-9}	0.23	0.10	2.64×10^{-6}	1.54×10^{-6}
Cr	0.00428	0.00183	2.83×10^{-7}	1.65×10^{-7}	1.43	0.61	4.71×10^{-4}	2.75×10^{-4}
HI	-	-	-	-	29.55	12.65	3.33×10^{-3}	1.95×10^{-3}

The values ADD, HQ and HI represent the average values of the average daily doses.

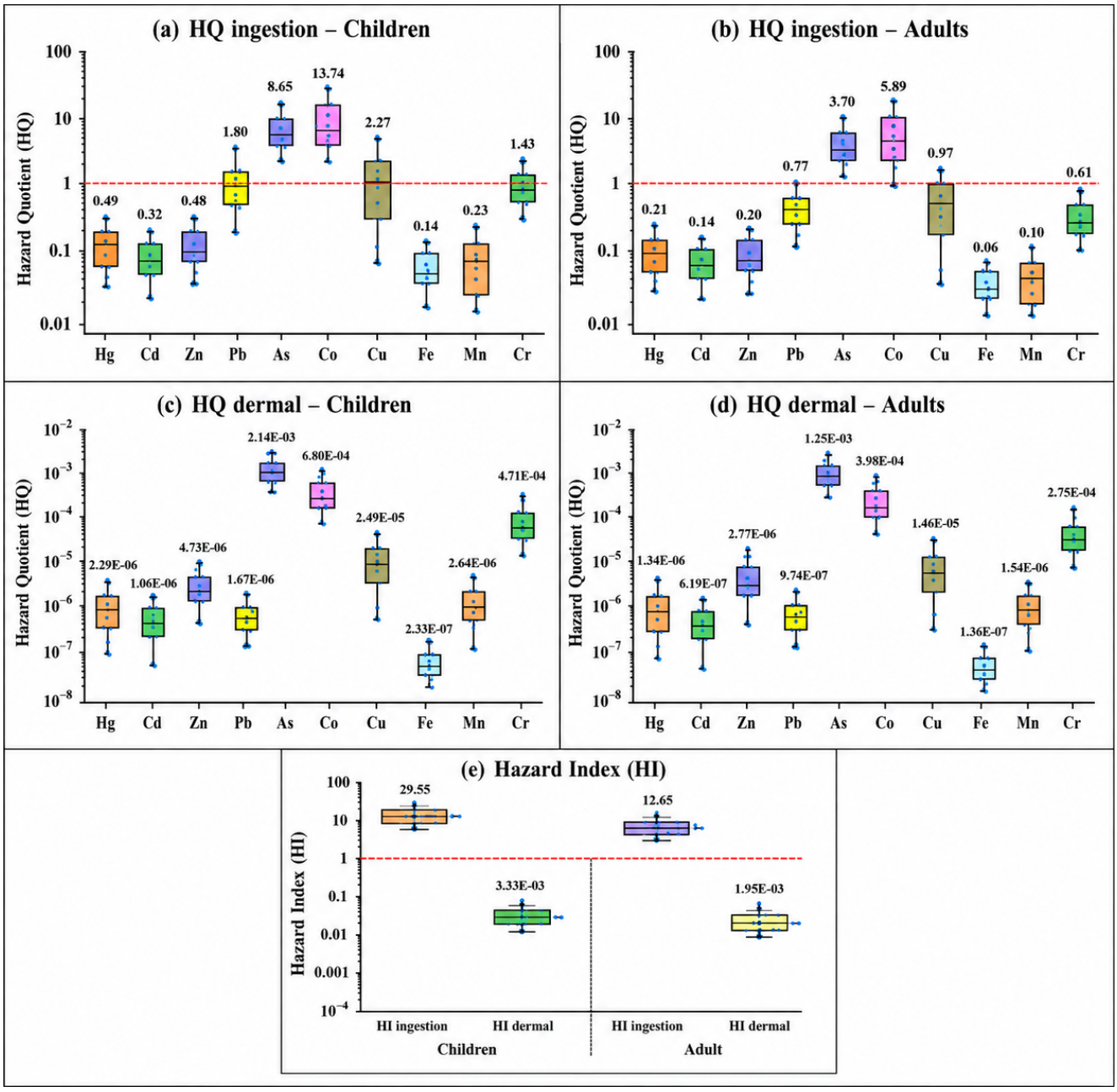

Figure 6. Box chart: (**a**) HQ ingestion in children; (**b**) HQ ingestion in adults; (**c**) HQ dermal in children; (**d**) HQ dermal in adults; and (**e**) HI.

5. Discussion

5.1. Disturbance-Recovery Continuum in a Tropical Mining Landscape

The exceptionally low dissolved oxygen (DO) value observed in one river sample may reflect a localized and temporary condition, such as increased oxygen demand, organic matter inputs, or metal oxidation processes. The relatively higher DO at mine sites (up to 86.1%) reflects turbulent flow in washing pools and temporary water agitation during mining activities, which re-aerates the water. This inverse relationship between DO and heavy metal concentrations implies that oxygen depletion

facilitates metal mobility by maintaining reducing conditions in sediments.

The acidity of the water may be linked to mining activities, particularly the oxidation of sulfide minerals (such as pyrite and arsenopyrite) exposed during excavation and the accumulation of waste rock. This process can generate acidic runoff and promote the release of potentially toxic elements into surrounding waterways [33]. Mining operations can raise water temperatures through deforestation, disturbance of water flow, or direct discharge of heated effluents. Increased temperatures reduce dissolved oxygen, thereby stressing aquatic life. On the other hand, high Pb and Zn contents are responsible for the basic nature of the water.

Suspended solids concentrations are low compared to those most often observed in forested and peri-urban watercourses [34]. Indeed, this low value of suspended particles might be linked to deforestation which reduces leaf fall, particularly in mining sites. The variation pattern of turbidity was similar to that of suspended solids, with higher values generally observed in the same sampling environments. This similarity reflects the contribution of suspended particulate matter to water turbidity. The higher values obtained in rivers are due to suspended particles from tree leaf debris. The Total Dissolved Solids show the highest concentrations in water from the mining sites, indicating that dissolved minerals and metals are introduced into water from mining operations. In fact, high TDS in water affects its taste, suitability for irrigation and aquatic life due to increased ion concentrations. High sediment loads degrade water clarity, impairing light penetration and harming aquatic life [35].

Unlike streams and rivers [34], the dissolved oxygen saturation rate is low, particularly in mining sites. Indeed, the decline in oxygen in the water would result from the oxidation of metals and the presence in suspension of oxygen-consuming elements.

The Water Quality Index (WQI) values decrease systematically from active mines (e.g., Pombe: 280.7, very poor) to abandoned mines (e.g., Njok: 85.6, good). This spatial pattern, when interpreted as a chronosequence, suggests progressive natural recovery of water quality following the cessation of mining activities. The usefulness of composite water-quality indices for identifying spatial patterns of pollution and linking water-quality degradation to anthropogenic inputs has also been demonstrated in other tropical and subtropical surface-water systems [36]. Similarly, the integration of water-quality indices with multivariate statistical and data-driven approaches has been shown to improve the assessment and prediction of spatial variations in surface-water quality [37]. In the present study, the observed improvement in WQI downstream of abandoned mining sites may reflect a combination of dilution by seasonal rainfall, sorption of metals onto secondary Fe/Mn oxyhydroxides abundant in ferralitic soils, and phytostabilization associated with vegetation recolonization (Figure 2). In contrast to some arid mining environments, where limited precipitation and slow weathering can prolong tailings persistence, tropical climates may enhance weathering, organic matter accumulation, and vegetation establishment. Nevertheless, reclamation outcomes in temperate regions are heterogeneous and depend on site-specific ecological, geochemical, and management conditions [38].

5.2. Mechanistic Controls on Metal Mobility

Gold mining increases the content of heavy metals in the surrounding environment. This occurs through various processes and activities associated with mining operations. Otherwise, water is the most important transport pathway of metals and metalloids resulting from the weathering of rocks, especially in humid tropical environments. In such environments, leaching from high pollution areas leads to high contamination by toxic heavy metals beyond the areas of anthropogenic activities (urbanization, mining and agricultural activities) [39]. Thus, water samples taken from watercourses, mine sites, and wells show much similarity in the semi-industrial gold mining area of Eséka.

The relatively high Pb concentration is certainly linked to anthropogenic inputs such as batteries and other electrical devices, pigments, fuels and paints, alloys and solders, pesticides and herbicides [40]. The extreme value at the Pombe site (0.55 mg/L) suggests a point source, likely galena (PbS) weathering or leakage of fuel/lubricants from excavation machinery. The lower but still elevated Pb in rivers indicates downstream dispersion. Critically, the abandoned Njok mine site showed much lower Pb (0.02 mg/L), approaching the WHO limit, suggesting natural attenuation over 5–10 years via adsorption onto Fe-Mn oxyhydroxides or burial under sediment. Furthermore, the high Pb and Cd contents are likely due to the presence of their common carrier minerals such as galena and sphalerite [41]. Additionally, cadmium exhibits very high solubility [42]. Conversely, high concentrations of Cr, Cd and As could be linked to the discharge of dissolved elements from ancient waste dumps [43]. High As contents pose significant danger to living organisms [44]. The elevated As at active mines is mechanistically linked to arsenopyrite (FeAsS) oxidation, a reaction accelerated by tropical temperatures (mean 27 °C) and mechanical crushing during gold recovery. The presence of As in well water is particularly concerning, indicating that dissolved As (as H_3AsO_4 or $H_2AsO_4^-$) migrates through permeable ferralitic soils into groundwater. The lower As in rivers suggests dilution or sorption onto suspended Fe(III) oxyhydroxides, which precipitate as yellow-brown coatings observed on streambeds. This trend implies that fluvial transport partially attenuates As, but groundwater remains at risk [45].

 https://doi.org/10.53941/ges.2026.100024

The main source of chronic arsenic poisoning worldwide appears to be groundwater, which can naturally contain elevated As concentrations in many regions. In contrast, arsenic-rich surface waters are commonly associated with mining environments where the oxidative weathering of As-bearing sulfide minerals, particularly arsenopyrite, promotes As release into drainage waters [46]. The elevated concentrations of Fe, Mn, Cr, Co, and Cu likely reflect a combination of the geochemical composition of the parent material and mining-related redistribution, as mining activities may enhance the mobilization and transport of metal-bearing minerals. Similar studies of surface-water systems have shown that the assessment of metal concentrations, hydrochemical facies, and water-quality indices can help distinguish the relative influence of natural geochemical processes and anthropogenic pressures on water quality [47]. In the present study area, these elements may also derive from natural sources, given their abundance in the underlying gneisses, amphibolites, and associated ferrallitic soils [7,48]. Leaching from surrounding soils into irrigation and surface waters may further contribute to their occurrence.

The high concentrations of some trace metals in rivers are probably linked to the discharge of effluents into nature following the treatment of gold by polluting chemical processes. This can also be explained by the leaching and dispersion of soluble elements contained in the dumps [44]. The dumps left uncovered are soaked and leached by rainwater which could carry dissolved materials rich in As, Cd and Mo into the watercourse. The high As and Fe concentrations (mean 0.06 and 1.33 mg/L at mine sites, respectively) are consistent with the oxidative dissolution of sulfide minerals (principally arsenopyrite (FeAsS) and pyrite (FeS2)) present in the local gneiss-hosted gold deposits. The relevant weathering reaction (e.g., for arsenopyrite) is [49]:

$$4FeAsS(s) + 11O_2(aq) + 6H_2O(l) \rightarrow 4Fe^{2+}(aq) + 4H_3AsO_3(aq) + 4SO_4^{2-}(aq)$$

This reaction is thermodynamically favored in warm (mean 27.2 °C), well-oxygenated surface waters and is accelerated by mechanical crushing during ore processing. The co-occurrence of Pb and Cd (CF up to 55.0 and 2.63, respectively) reflects the weathering of co-crystallized galena (PbS) and sphalerite (ZnS), which commonly host Cd as a trace impurity [50].

The elements Cu, Mn, Fe, and As appear to originate from a common source or to be remobilized through similar geochemical processes, as reported in several case studies conducted in Cameroon [51–53]. Thus, As is likely derived primarily from an anthropogenic source, whereas Zn and Cd are considered to have a natural origin [54]. Although Pb is not associated with As, no natural source of Pb has been identified in the surface waters of the study area. Furthermore, the pH values, together with the elevated concentrations of As and Cd, appear to contribute to the increase in surface-water temperature.

5.3. Impact of Heavy Metals on Human Health

The health risk assessment indicates that ingestion is the predominant potential exposure pathway for local populations. HQ and HI values above the threshold of 1 suggest potential non-carcinogenic risks for children exposed to Zn, Pb, As, Co, Cu, Fe, Mn, and Cr, whereas adults showed potential risks only for As and Co. Similar findings have been reported in recent studies conducted in mining-impacted areas, where children generally exhibited higher non-carcinogenic risks than adults and ingestion was identified as the dominant exposure pathway [55,56]. In particular, Kazapoe et al. [55] reported HI values above 1 for As, Cr, Co, and V among children in a mining area in southwestern Ghana, while ingestion was identified as the primary exposure route. These results highlight the greater vulnerability of children due to their physiological characteristics and exposure-related behaviors [55,57]. Similar risk-assessment approaches have been applied in mining environments, where the combined evaluation of environmental contamination, exposure pathways, hazard indices, and uncertainty has been used to identify areas requiring targeted intervention [55,56,58]. However, the estimated risks are derived from standard exposure models and represent potential rather than actual health effects. Moreover, recent studies have emphasized that uncertainty in exposure parameters and risk-model assumptions can substantially influence the resulting risk estimates [55,58].

Dermal exposure posed negligible health concern, as all HQ and HI values remained below 1, confirming that ingestion is the dominant exposure pathway in the present study. This observation is consistent with recent evidence from mining-affected soils, where ingestion was reported as the principal exposure route for both adults and children [55]. The ranking of mean HQ values identified Co and As as the primary contributors to potential health risks, followed by Cu, Pb, and Cr, while Fe showed the lowest contribution. The importance of As and other potentially toxic elements as major contributors to health risks has also been reported in recent mining studies [55,59]. Children exhibited a mean HI value of 29.55 for ingestion, compared with 12.65 for adults, corresponding to a value approximately 2.34 times higher in children. This greater susceptibility of children may be attributed to their lower body weight and frequent hand-to-mouth activity and is consistent with recent health-risk assessments conducted in mining areas, which have reported higher non-carcinogenic risks among children than adults [55,57]. It should be noted that uncertainties remain due to assumptions regarding exposure parameters and because the assessment is

based on total metal concentrations rather than their site-specific bioavailability. Indeed, recent studies have demonstrated that risk assessments based solely on total metal(loid) concentrations may overestimate toxicological risks, whereas consideration of bioavailable and bioaccessible fractions can provide a more realistic estimate of potential human health risks [60,61]. Similar concerns regarding the influence of bioavailability and bioaccessibility on risk characterization have been reported in contaminated and mining-affected soils [60–62].

5.4. Study Limitations and Future Work

Despite the novel insights provided by this study on the disturbance-recovery continuum in a tropical mining landscape, several limitations must be acknowledged, which also define priorities for future research. First, the dataset is derived from a single field campaign (dry season) with a limited number of samples (n = 10). While this snapshot effectively captures spatial variability across active and abandoned sites, it cannot resolve temporal dynamics, particularly seasonal fluctuations in water chemistry driven by contrasting hydrologic regimes (e.g., wet season dilution vs. dry season concentration). Future work should implement a multi-seasonal monitoring program to quantify the role of rainfall intensity, surface runoff, and groundwater recharge in modulating metal mobilization and attenuation. Second, the interpretation of natural restoration relies on a space-for-time substitution. Direct validation through repeated sampling of the same sites over a decade would be required to confirm the inferred recovery trajectory. Finally, while we propose sulfide oxidation and sorption onto Fe oxyhydroxides as the dominant mechanisms controlling metal mobility, direct mineralogical evidence (e.g., X-ray diffraction of suspended sediments, scanning electron microscopy on waste rock surfaces) is lacking. Future work should couple aqueous geochemistry with solid-phase characterization to close the mass balance and validate the proposed reaction pathways. Addressing these limitations will transform the current pilot study into a robust, mechanistic understanding of how semi-industrial mining interacts with tropical Earth surface processes; information that is urgently needed to guide sustainable mining practices and remediation policies across Central Africa and analogous regions globally.

6. Conclusions

Surface water from the Eséka gold district (Central Cameroon) was analyzed to assess the environmental influence of semi-industrial gold mining. The main conclusions are as follows:

- The Eséka gold district exhibits a clear disturbance gradient, with active mining sites showing degraded water quality, whereas some abandoned sites, such as Njok (~5–10 years after abandonment), display signs of natural recovery. However, this recovery is site-dependent and does not necessarily indicate the complete removal of metal contamination, as water quality indices may remain compatible with good status while specific trace elements exceed guideline values.
- Metal mobilization is likely associated with the weathering and oxidation of sulfide-bearing minerals (e.g., arsenopyrite and pyrite), processes enhanced by humid tropical conditions. Natural attenuation may occur through adsorption onto secondary Fe minerals and ecosystem recolonization, but its effectiveness varies according to local geochemical and hydrological conditions.
- From a health perspective, ingestion of surface water represents the main exposure pathway, with potential non-carcinogenic risks (HI > 1) mainly related to Pb, As, Co, and Cr for children and As and Co for adults, whereas dermal exposure contributes negligibly.
- This study highlights the importance of combining geochemical assessment, risk evaluation, and long-term monitoring to understand post-mining trajectories in tropical environments. Management strategies should include regular monitoring of abandoned mining sites, community awareness programs regarding the risks of using mining-affected waters for irrigation, and progressive implementation of active remediation measures where natural recovery processes are insufficient.

Author Contributions

I.G.A.: conceptualization, methodology, software; M.W.: data curation, writing—original draft preparation; R.D.T.: visualization, investigation; E.S.: software, validation, writing—reviewing and editing; V.L.O.: draft review and supervision. All authors have read and agreed to the published version of the manuscript.

Funding

This research received no external funding.

Institutional Review Board Statement

Not applicable.

Informed Consent Statement

Not applicable.

Data Availability Statement

Data are available from the corresponding author upon reasonable request.

Acknowledgments

We are grateful to the Editor and anonymous reviewers for improving the final manuscript.

Conflicts of Interest

The authors declare no conflict of interest.

Use of AI and AI-Assisted Technologies

Generative AI tools, namely ChatGPT and DeepL Write, were used solely to improve the language, grammar, clarity, and readability of the manuscript. Their use was limited to language editing and linguistic polishing. No AI tools were used for content generation, data analysis, interpretation, or the formulation of scientific conclusions. The authors take full responsibility for the content and integrity of the manuscript.

References

1. FAO. *Water Overview*; Food and Agriculture Organization of the United Nations: Rome, Italy, 2026.
2. Normatov, P.; Armstrong, R.; Normatov, I.; et al. Monitoring extreme water factors and studying the anthropogenic load of industrial objects on water quality in the Zeravshan River basin. *Russ. Meteorol. Hydrol.* **2015**, *40*, 347–354.
3. Salvarredy Aranguren, M.M. Contamination en métaux lourds des eaux de surface et des sédiments du Val de Milluni (Andes boliviennes) par des déchets miniers: Approches géochimiques, minéralogiques et hydrochimiques. Ph.D. Thesis, Université Toulouse III–Paul Sabatier, Toulouse, France, 2008; 371p + 86p.
4. Singh, V.; Singh, N.; Rai, S.N.; et al. Heavy metal contamination in the aquatic ecosystem: toxicity and its remediation using eco-friendly approaches. *Toxics* **2023**, *11*, 147.
5. Ngoa Manga, E.S.; Ekoa Bessa, A.Z.; Ayissi Mbomo, R.E.; et al. Evaluation of surface water contamination and its impacts on health in the mining districts of Kambélé and Bétaré-Oya (Eastern-Cameroon). *Heliyon* **2024**, *10*, e29189.
6. Sababa, E.; Ndong Bidzan, F.; Thena, N.; et al. Evaluation des éléments traces métalliques (Cr, As, Pb, Zn et Cd) dans les eaux de surface du bassin versant du Lom, Est Cameroun: Impact de l'exploitation semi-industrielle de l'or. *Sci. Technol. Dev.* **2018**, *20*, 1–10.
7. Sababa, E.; Mbesse, C.O.; Wandji Mouko, C.N.; et al. Geochemistry of stream sediments from Eséka area (SW Cameroon): implications for surface process assessment and precious metals (Au, Pd, and Pt) exploration. *J. Sediment. Environ.* **2022**, *7*, 43–66.
8. Atangana, M.S.B.; Ndam Ngoupayou, J.R.; Deliege, J.F. Hydrogeochemistry and Mercury Contamination of Surface Water in the Lom Gold Basin (East Cameroon): Water Quality Index, Multivariate Statistical Analysis and Spatial Interpolation. *Water* **2023**, *15*, 2502.
9. Kouankap Nono, G.D.; Tah Bong, C.; Wotchoko, P.; et al. Artisanal gold mining in Batouri area, East Cameroon: Impacts on the mining population and their environment. *J. Geol. Min. Res.* **2017**, *9*, 1–8.
10. Mambou Ngueyep, L.L.; Takougang Kingni, S.; Ayiwouo Ngounouno, M.; et al. The impact of gold mining exploitation on the physicochemical quality of water: case of Batouri (Cameroon). *Int. J. Energy Water Resour.* **2021**, *5*, 159–173.
11. Rakotondrabe, F.; Ngoupayou, J.R.N.; Mfonka, Z.; et al. Assessment of surface water quality of Bétaré-Oya gold mining area (East-Cameroon). *J. Water Resour. Prot.* **2017**, *9*, 960–984.
12. Owona, S.; Schulz, B.; Minyem, D.; et al. Eburnean/Trans-Amazonian orogeny in the Nyong complex of southwestern Cameroon: Meta-basite geochemistry and metamorphic petrology. *J. Afr. Earth Sci.* **2022**, *190*, 104515.
13. Feybesse, J.L.; Johan, V.; Maurizot, P.; et al. Evolution tectonométamorphique libérienne et éburnéenne de la partie NW du craton zaïrois (SW Cameroun). In Proceedings of the 14th Colloquium on African Geology, Berlin, Germany, 18–22 August 1987; pp. 9–12.
14. Toteu, S.F.; Penaye, J.; Djomani, Y.P. Geodynamic evolution of the Pan-African belt in central Africa with special reference to Cameroon. *Can. J. Earth Sci.* **2004**, *41*, 73–85.
15. Champetier de Ribes, G.; Aubague, M. *Carte Géologique de Reconnaissance à l'echelle du 1/500000*; Royal Museum for Central Africa: Tervuren, Belgium, 1956; 35p.
16. Eymery, F.; Choubert, J.; Lepot, B.; et al. *Guide Technique OpéRationnel: Pratiques D'éChantillonnage Et De Conditionnement en Vue De La Recherche De Micropolluants Prioritaires Et éMergents en Assainissement Collectif Et Industriel*, Première version ed.; Irstea/Cemagref: Lyon, France, 2011; 85p.
17. American Public Health Association (APHA). *Standard Methods for the Examination of Water and Sewage*; American Public Health Association: Washington, DC, USA, 1912. pp. 11–15.
18. Rodier, J.; Legube, B.; Merlet, N. *L'analyse De L'eau*, 9th ed.; Dunod: Paris, France, 2009; 1579p.
19. N'guessan, Y.M.; Wango, T.E.; Adopo, K.L.; et al. Geochemical characteristics of surface waters in an agricultural environment: Case of Gascogne catchments (Midi Pyrénées Region, S-W France). *Int. J. Innov. Appl. Stud.* **2016**, *17*, 394–406.
20. Horton, R.K. An index number system for rating water quality. *J. Water Pollut. Control Fed.* **1965**, *37*, 300–306.
21. Brown, R.; McClelland, N.; Deininger, R.; et al. A water quality index—Do we dare? *Water Sew. Work.* **1970**, *117*, 339–343.
22. WHO. *Guidelines for Drinking-Water Quality*, 4th ed.; World Health Organization: Geneva, Switzerland, 2011; 518p.
23. Sahu, P.; Sikdar, P.K. Hydrochemical framework of the aquifer in and around East Kolkata Wetlands, West Bengal, India. *Environ. Geol.* **2008**, *55*, 823–835.

24. Asomaku, S.O. Quality assessment of groundwater sourced from nearby abandoned landfills from Industrial City in Nigeria: Water pollution indices approach. *HydroResearch* **2023**, *6*, 130–137.
25. Mohan, S.V.; Nithila, P.; Reddy, S.J. Estimation of heavy metals in drinking water and development of heavy metal pollution index. *J. Environ. Sci. Health. Part A Environ. Sci. Eng. Toxicol.* **1996**, *31*, 283–289.
26. Ojekunle, O.Z.; Ojekunle, O.V.; Adeyemi, A.A.; et al. Evaluation of surface water quality indices and ecological risk assessment for heavy metals in scrap yard neighbourhood. *SpringerPlus* **2016**, *5*, 560.
27. Okanlawon, M.O.; Olasehinde, P.I.; Abdullahi, I.N.; et al. Water quality determination around gold and manganese mining area using metal pollution index and water quality index in South-Western part of Tegina Sheet 142 North Central Nigeria. *Int. J. Innov. Res. Dev.* **2017**, *6*, 40–49.
28. Hakanson, L. An ecological risk index for aquatic pollution control. A sedimentological approach. *Water Res.* **1980**, *14*, 975–1001.
29. Tomlinson, D.L.; Wilson, J.G.; Harris, C.R.; et al. Problems in the assessment of heavy-metal levels in estuaries and the formation of a pollution index. *Helgoländer Meeresunters.* **1980**, *33*, 566–575.
30. Khan, S.; Cao, Q.; Zheng, Y.; et al. Health risks of heavy metals in contaminated soils and food crops irrigated with wastewater in Beijing, China. *Environ. Pollut.* **2008**, *152*, 686–692.
31. Cabrera, F.; Clemente, L.; Díaz Barrientos, E.; et al. Heavy metal pollution of soils affected by the Guadiamar toxic flood. *Sci. Total Environ.* **1999**, *242*, 117–129.
32. US-EPA (United States Environmental Protection Agency). *Risk Assessment: Regional Screening Levels (RSLs)—Equations*; US-EPA: Washington, DC, USA, 2023; pp. 1–6.
33. Mall, I.; Diaw, M.; Dieng, N.M.; et al. Evaluation of water resources quality in Sabodala gold mining region and its surrounding area (Senegal). *J. Water Resour. Prot.* **2015**, *7*, 247–263.
34. Foto Menbohan, S.; Tchakonte, S.; Ajeagah Gideon, A.; et al. Water quality assessment using benthic macroinvertebrates in a periurban stream (Cameroon). *Int. J. Biotechnol.* **2013**, *2*, 91–104.
35. Davies-Colley, R.J.; Smith, D.G. Turbidity suspended sediment, and water clarity: A review. *J. Am. Water Resour. Assoc.* **2001**, *37*, 1085–1101.
36. Sababa, E.; Ekoa Bessa, A.Z. Heavy Metals Signature in Stream Sediments at Eséka Gold District, Central Africa: A Pre-mining Environmental Assessment. *Chem. Afr.* **2022**, *5*, 413–430.
37. Al-Falal, A.N.A.; Elsayed, S.; El Fadaly, E.A.; et al. Aquatic system assessment of potentially toxic elements in El Manzala Lake, Egypt: A statistical and machine learning approach. *Results Eng.* **2025**, *26*, 105027.
38. Byrne, P.; Yendell, A.; Frau, I.; et al. Identification and prioritisation of mine pollution sources in a temperate watershed using tracer injection and synoptic sampling. *Mine Water Environ.* **2021**, *40*, 980–993.
39. Abende Sayom, Y.R.; Mefomdjo, B.F.; Tarkwa, J.B.; et al. Comprehensive Water Quality and Heavy Metal Pollution Assessment of the Lom River in Bekao Gold Mining Sites (Adamawa-Cameroon) Using the Pollution Indices and Multivariate Statistical Approach. *Water Air Soil Pollut.* **2023**, *234*, 653.
40. Samba Assomo, P.; Bouba, L.; Kouayep Lawou, S.; et al. Physico-chemical characterization and metallic trace element concentrations in surface waters of East Cameroon: case studies of the Tidamba watercourse in Bertoua and the Kambele mining basin in Batouri. *Arab. J. Geosci.* **2023**, *16*, 252.
41. Sparks, D.L. Fundamentals of soil chemistry. In *Encyclopedia of Water: Science, Technology, and Society*; John Wiley & Sons, Inc.: Hoboken, NJ, USA, 2019; pp. 1–11.
42. Wong, H.K.T.; Gauthier, A.; Nriagu, J.O. Dispersion and toxicity of metals from abandoned gold mine tailings at Goldenville, Nova Scotia, Canada. *Sci. Total Environ.* **1999**, *228*, 35–47.
43. Yang, M.; Fu, W.; Chen, H.; et al. The impacts of molybdenum exploration on Cd and Zn contents in surface water: Evidence from a molybdenum mine in the Xiaoqinling Mountains. *Minerals* **2023**, *13*, 1207.
44. Serfor-Armah, Y.; Nyarko, B.J.B.; Dampare, S.B.; et al. Levels of Arsenic and Antimony in Water and Sediment from Prestea, A Gold Mining Town in Ghana and its Environs. *Water Air Soil Pollut.* **2006**, *175*, 181–192.
45. Mefomdjo Fotie, B.; Boukari, H.; Daou, I.E.; et al. Physicochemical Characterisation of Water and Sediment of the Semimechanized Artisanal Gold Mining Environment of the Béké Locality. *Appl. Environ. Soil Sci.* **2024**, *2024*, 6888252.
46. Corkhill, C.L.; Vaughan, D.J. Arsenopyrite oxidation—A review. *Appl Geochem.* **2009**, *24*, 2342–2361.
47. Gad, M.; Saleh, A.H.; Hussein, H.; et al. Appraisal of surface water quality of Nile River using water quality indices, spectral signature and multivariate modeling. *Water* **2022**, *14*, 1131.
48. Nga Essomba Tsoungui, P.; Ganno, S.; Tanko Njiosseu, E.L.; et al. Geochemical constraints on the origin and tectonic setting of the serpentinized peridotites from the Paleoproterozoic Nyong series, Eséka area, SW Cameroon. *Acta Geochim.* **2020**, *39*, 404–422.
49. Appleton, J.; Williams, T.; Orbea, H.; et al. Fluvial contamination associated with artisanal gold mining in the Ponce Enriquez, Portovelo-Zaruma and Nambija areas, Ecuador. *Water Air Soil Pollut.* **2001**, *131*, 19–39.
50. George, L.L.; Cook, N.J.; Ciobanu, C.L.; et al. Partitioning of trace elements in co-crystallized sphalerite–galena–chalcopyrite hydrothermal ores. *Ore Geol. Rev.* **2016**, 77, 97–116.
51. Ndema Mbongué, J.L.; Sigué, C.; Mbowou Ngantche, I.F.; et al. Potentially toxic metals contamination in stream

sediments of Mbal area (Pan-African fold belt, Cameroon). *Discov. Geosci.* **2024**, *2*, 15.

52. Dairou, B.; Ngo Bidjeck Bondje, L.M.; Ndjigui, P.D. Assessment of pollution and ecological risk associated with heavy metals in sediments from the rivers of Batouri gold mining area (East Cameroon): geochemical and statistical approaches. *J. Sediment. Environ.* **2025**, *10*, 159–171.
53. Diab, D.A.; Marcel, J.; Aguiza Abai, E.; et al. Hydrogeological Impact of Gold Mining, Contaminant Flow Patterns and Groundwater Quality Assessment in the Kambele Mining Area, Eastern Part of Cameroon. *J. Environ. Prot.* **2025**, *16*, 384–402.
54. Ayiwouo, M.N.; Yamgouot, F.N.; Mambou, L.L.N.; et al. Impact of gold mining on the water quality of the Lom River, Gankombol, Cameroon. *Heliyon* **2022**, *8*, e12452.
55. Kazapoe, R.W.; Kwayisi, D.; Alidu, S.; et al. Source-specific probabilistic health risk assessment of potentially toxic elements in soils from a mining area using Monte Carlo simulation: A case study from southwestern Ghana. *Ecol. Indic.* **2025**, *174*, 113376.
56. Sun, L.; Wang, X.; Liu, Y.; et al. Improved model for human health risk assessment of soil heavy metal(loid)s in a mining area of southeastern China. *Ecotoxicol. Environ. Saf.* **2025**, *306*, 119312.
57. Yu, J.; Li, J.J.; Han, R.B.; et al. Health Risk Assessment of Heavy Metals in Mining Soils and Analysis of Influencing Factors. *Huan Jing Ke Xue* **2026**, *47*, 1316–1328.
58. Yuan, B.; Du, P.; Chen, J.; et al. Two-dimensional Monte Carlo simulation improves source-specific health risk assessment accuracy of soil heavy metals in a legacy mining region. *J. Hazard. Mater.* **2025**, *496*, 139190.
59. Zhou, Y.; Ding, D.; Li, X.; et al. The integrating eco-health risk assessment and driving factors for risks of heavy metals in soils from an open-pit lead-zinc mine area. *Ecotoxicol. Environ. Saf.* **2026**, *321*, 120348.
60. Li, H.; Yao, J.; Min, N.; et al. Considering the bioavailability and bioaccessibility of metal(loid)s for risk assessment of soils affected by different non-ferrous metal activities in Southwest China. *J. Hazard. Mater.* **2024**, *472*, 134527.
61. Liu, S.; Li, Y.; Zhan, C.; et al. Assessing bioavailability risks of heavy metals in polymetallic mining regions: A comprehensive analysis of soils with varied land uses. *Environ. Monit. Assess.* **2024**, *196*, 975.
62. Ata, A.A.E.S.M.; Aly, M.H.; Hussein, H.; et al. Hydrogeochemical characteristics and air quality risks associated with gold mining operations in Egypt using geochemical modeling and risk indices. *Heliyon* **2024**, *10*, e31086.